Vortex solid-solid transition in a $Bi_{1.6}Pb_{0.4}Sr_2CaCu_2O_{8+\delta}$ crystal

M. Baziljevich,[1,2] D. Giller,[1] M. McElfresh,[1,3] Y. Abulafia,[1] Y. Radzyner,[1] J. Schneck,[4] T. H. Johansen,[2] and Y. Yeshurun[1]
[1]*Institute of Superconductivity, Department of Physics, Bar-Ilan University, 52900 Ramat Gan, Israel*
[2]*Department of Physics, University of Oslo, P.O. Box 1048, Blindern 0316, Oslo, Norway*
[3]*Department of Physics, Purdue University, West Lafayette, Indiana 47907*
[4]*France Telecom–CNET Laboratorie de Bagneux, BP 107, 92225 Bagneux Cedex, France*
(Received 8 February 2000)

The magnetic vortex phase diagram of $Bi_{1.6}Pb_{0.4}Sr_2CaCu_2O_{8+\delta}$ was measured using a Hall sensor array. Pb doping was shown to drastically change the magnetic phase diagram including a significant increase in the irreversibility field and a temperature dependence of the onset field of the second magnetization peak. Anisotropy was determined using a recently proposed scaling expression, which relates the anisotropy to the irreversibility line. Based on the obtained anisotropy an excellent fit of the experimental $B_{on}(T)$ data to the model of disorder-induced transition was found for three basic regimes: $L_c<s<L_0$ for $T<48$ K, $s<L_c<L_0$ for $48<T<66$ K, and $s<L_0<L_c$ for $T>66$ K, where s, L_0, and L_c are, respectively, the interlayer spacing, the characteristic size of the longitudinal fluctuations in a cage, and the size of a coherently pinned vortex segment.

I. INTRODUCTION

The magnetic phase diagram associated with the magnetic vortex matter states in high-temperature superconductors (HTS's) is a topic of extensive theoretical and experimental research. Recently, a great deal of effort has been focused on highly anisotropic $Bi_2Sr_2CaCu_2O_{8+\delta}$ (BSCCO), revealing a rich phase diagram. Neutron-scattering[1] and muon spin rotation[2] experiments have revealed the existence of two distinct vortex solid phases: a quasiordered lattice at low fields and a highly disordered solid at high fields. The transition between these two phases is manifested in magnetic measurements as a sharp increase in the magnitude of the magnetization resulting from an increase in the persistent current density.[3–8] This second peaking of the magnetization as a function of applied field, or ''fishtail,'' was also observed in a variety of HTS's and low-temperature superconductor (LTS) materials, such as $YBa_2Cu_3O_{7-\delta}$ (YBCO),[9–11] $Nd_{1.85}Ce_{0.15}CuO_{4-\delta}$ (NCCO),[12] $(La_{1-x}Sr_x)_2CuO_4$ (LSCO),[13] Tl-based compounds (TBCCO),[14–16] Hg-based compounds (HBCO),[15,17] $CeRu_2$,[18] $NbSe_2$,[19,20] and Nb.[21] While the peak field of the fishtail is time dependent, and has been shown to be consistent with a crossover from an elastic to a plastic flux creep mechanism,[10,16,17,20,22,23] the onset of the fishtail appears to be associated with a transition between the two solid phases at the field B_{on}.

A recent model[24–26] associates this transition with a disorder induced transition. In this model, the transition field is determined by a competition between the vortex elastic energy $E_{elastic}$ and the pinning energy $E_{pinning}$. Both of these energies depend on the magnetic penetration depth λ and the coherence length ξ, and hence on field and temperature. At low fields the elastic interactions govern the structure of the vortex solid leading to the formation of a quasiordered lattice. At fields above B_{on}, however, disorder dominates and vortex interactions with pinning centers result in an entangled solid where cells of the vortex lattice are twisted and dislocations proliferate. According to this approach, the line $B_{on}(T)$ is the crossing line of the two surfaces $E_{elastic}(B,T)$ and $E_{pinning}(B,T)$. By employing this approach it is possible to explain the details of the transition line $B_{on}(T)$ in several systems,[11] including BSCCO, NCCO, and YBCO, despite the large differences in their T_c values, the range of fields and temperatures for which this anomaly is observed, and the pronounced difference in the temperature dependence of B_{on} in these systems.

Another parameter, which plays an important role in determining the elastic and the pinning energies, is the anisotropy γ. It is expected that by controlling the anisotropy, B_{on} will be affected. Indeed, as shown by Khaykovich *et al.*[7] and Ooi, Tamegai, and Shibauchi,[27] the transition line $B_{on}(T)$ for BSCCO, underdoped or overdoped with oxygen, is markedly different from the line measured for optimally doped BSCCO. While the latter persists only up to 40 K, showing no temperature dependence in this range, in the overdoped and underdoped samples B_{on} persists up to the vicinity of T_c, exhibiting a decrease to zero close to this temperature. Though the details of $B_{on}(T)$ in these samples have not been analyzed, it is clear that these results are qualitatively consistent with the predictions of the model described above.

In this work Pb doping is used to reduce the anisotropy of BSCCO.[29,30] Measurements of local magnetization are used to construct the magnetic phase diagram for this system. The anisotropy γ is estimated using the empirical equation introduced by Kitazawa *et al.*,[31] which relates the anisotropy to the measured irreversibility line at low temperatures. In Pb-doped BSCCO the onset field B_{on}, separating the two vortex solid phases, exhibits an unusual nonmonotonous temperature dependence with three distinct regimes. The estimated value of γ is used in a self-consistent calculation of $B_{on}(T)$ within the framework of the disorder-induced transition scenario. The effect of γ on both $E_{pinning}$ and $E_{elastic}$ is shown to be the main factor responsible for the different temperature dependences of B_{on} in pure and Pb-doped BSCCO.

II. EXPERIMENT

Single crystals were prepared by mixing powders of Bi_2O_3, PbO, CuO, $CaCO_3$, and $SrCO_3$.[32] The starting composition of the powders corresponds to an excess of Ca, Cu, and Pb with respect to the final compound $(Bi,Pb)_2Sr_2CaCu_2O_{8+\delta}$. The mixture is heated to 950 °C and kept there for 12 h. Depending on the Pb content of the mixture, this temperature exceeds the melting point by 80–110 K. The crystals grow during a slow cooling of the flux at a rate of 1 K per hour, where the temperature sweep is controlled to better than 0.1 K. After the growth is completed the crystals are cooled to room temperature at a rate determined by the thermal inertia of the furnace. During this slow cooling we expect that the oxygen concentration becomes uniform and reaches equilibrium via diffusion.

At room temperature the solidified flux consists of several crystalline species, where the $Bi_{2-x}Pb_xSr_2CaCu_2O_{8+\delta}$ single crystals are easily identified by their platelet shape and shiny appearance. The cation concentrations in these crystals were measured using an electron microprobe of 1 μm diameter, and found to be consistent with the 2:2:1:2 phase. Moreover, these measurements show that maximum solubility of Pb corresponds to the formula $Bi_{1.6}Pb_{0.4}Sr_2CaCu_2O_{8+\delta}$ [BSCCO (Pb=0.4)]. In this work Pb-free crystals, BSCCO (Pb=0), and maximally doped crystals, BSCCO (Pb=0.4), were chosen for the further investigations. Two single crystals, carefully selected from the batches, were cut with a wire saw to the dimensions $210\times780\times25$ μm^3 [BSCCO (Pb=0.4)], and $220\times940\times15$ μm^3 [BSCCO (Pb=0)]. In the low-field limit the BSCCO (Pb=0.4) sample has $T_c=95$ K with $\Delta T_c=4$ K, and the undoped BSCCO crystal has $T_c=90$ K with $\Delta T_c=10$ K. The T_c values of these crystals indicate that their oxygen content is close to optimum.[33]

The magnetic measurements were performed using the micro-Hall probe technique. An array consisting of $n=11$ GaAs/AlGaAs Hall sensors each with a 10×10-μm^2 active area and a 10-μm separation, allowed the measurement of spatial dependent profiles of the normal component of the magnetic induction $B_z(x_n)=B_n$ at the sample surface.[34] The field sensitivity with this technique is better then 0.1 G and fields up to 5 T can be detected. One of the probes is used to measure the external field by mounting the sample directly onto the array so that this probe is located outside the sample edge. The field is always applied perpendicular to the sample platelet which is parallel to the crystallographic c axis.

III. RESULTS

Hall-probe data can be conveniently analyzed by considering the difference between probe signals, $\Delta B_n=B_n-B_{n'}$, where the probe n' serves as reference. In some cases the reference signal is found by averaging the signal from two probes. Hysteresis loops are formed as ΔB_n is measured as a function of the applied field B_a. These hysteresis loops strongly resemble loops obtained from conventional magnetometry so it is customary to denote Hall probe data as local magnetization. This terminology will also be used here, although we are fully aware that local magnetization in the perpendicular field geometry is a different quantity.[35,36]

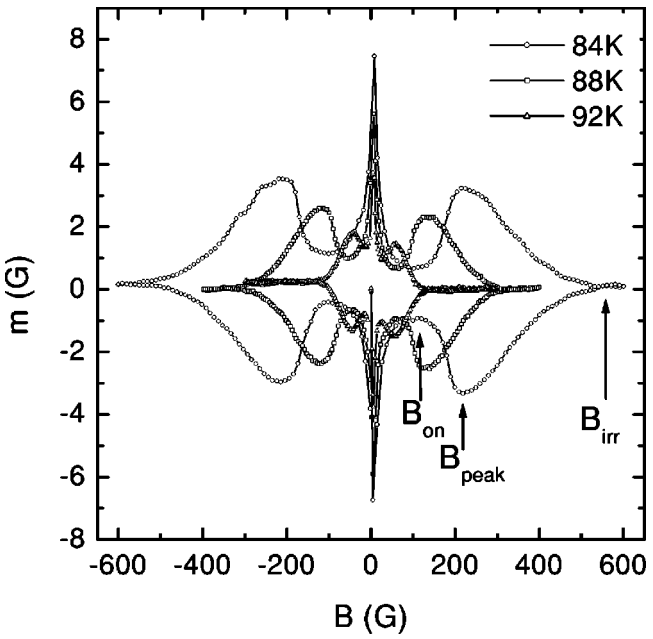

FIG. 1. Magnetization loops $m=B_4-B_{8,9}$ plotted against the local induction B_4, for the BSCCO (Pb=0.4) crystal at 84, 88, and 92 K.

Figure 1 shows typical magnetization loops $m=B_4-B_{8,9,}$ measured for the Pb-doped sample, plotted against the local induction B_4. Probe 4 is located close to the sample center, whereas $B_{8,9}$ is the average signal of probes 8 and 9 which are located close to the neutral line position.[37] At the neutral line B is approximately equal to the applied field B_a. The three loops in Fig. 1 were obtained at 84, 88, and 92 K illustrating the particular temperature dependence of the magnetization in this temperature range near T_c. The sample exhibits a distinct second peak, i.e., a strong increase in the magnitude of the magnetization in an intermediate field range. Experimentally one may define three characteristic fields which are indicated in the figure. The lowest of these is B_{on} denoting the onset field of the second peak while the peak maximum occurs at B_{peak}. The irreversibility field B_{irr} denotes the field where the $B(B_a)$ loop width is reduced to zero, i.e., below the noise level. The temperature dependence of these characteristic fields forms a phase diagram in the B-T plane.

The phase diagram obtained for the Pb-doped sample in the temperature range 15–92 K is presented in Fig. 2. All the fields B_{on}, B_{peak}, and B_{irr} are found to exist over this whole temperature interval. Between 25 and 70 K the value of B_{on} is approximately constant and then decreases rapidly together with the other characteristic fields as T approaches T_c. Below 25 K, B_{on} rapidly approaches the value of B_{peak}. This occurs because the magnitude of the full penetration field becomes comparable to the characteristic field of the second peak, eventually masking the fishtail effect at the lower temperatures.

The magnetic behavior of the BSCCO (Pb=0) crystal was investigated from 15 K and up to T_c. In this interval the second peak was observed only in a small temperature range between 20 and 30 K consistent with other reports,[7] how-

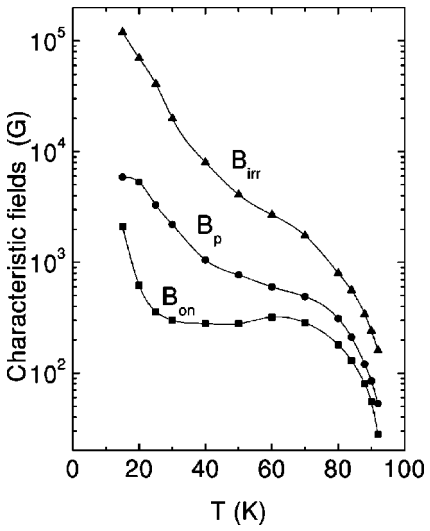

FIG. 2. Magnetic phase diagram defined by the fields B_{on}, B_{peak}, and B_{irr}, determined for the BSCCO (Pb=0.4) sample.

ever, the irreversibility field B_{irr} could be measured over the whole interval up to T_c. The values of B_{irr} and B_{peak} in the undoped sample are both an order of magnitude smaller than in the doped sample, while the values of B_{on} are comparable [in BSCCO (Pb=0), $B_{on}\sim 200$ G, independent of temperature]. In addition, the second peak is generally sharper in the undoped sample than in the Pb-doped sample. Whereas the ratio B_{peak}/B_{on} is close to 2 in BSCCO (Pb=0), it is on the order of 10 for the BSCCO (Pb=0.4) sample at the same temperature.

In order to investigate the dynamic behavior of the second peak, relaxation measurements were performed on the BSCCO (Pb=0.4) crystal. The initial state was prepared by zero-field cooling and subsequently applying a constant field B_a. The induction at each probe was then measured as a function of time. From the time-dependent induction profiles obtained with the probe array, the persistent current J was determined by a fitting procedure described elsewhere.[38] Figure 3 shows the relaxation of J with time at various B_a at 30 K. The upper $J(B_a)$ curve is obtained at $t=8$ seconds, where $t=0$ corresponds to the time when B_a is established. This curve displays a distinct second peak centered at 2.4 kG. As time evolves the peak in $J(B_a)$ is seen to gradually shift toward lower fields eventually reaching 1.9 kG, as seen in the lower curve of Fig. 3, at 650 sec. The relaxation behavior is different on the two sides of the peak, with the relaxation rate increasing with B_a up to the peak at B_{peak} and then the rate appearing essentially field independent above the peak.

The current density dependence of the local flux creep activation energy, $U(J)$, can be found using a recently developed method.[39] The analysis is based on the calculation of the flux current density D defined as

$$D(x,t)=-\int_0^x \frac{\partial B_z(x',t)}{\partial t}dx'. \tag{1}$$

Here $x=0$ corresponds to the sample center where $D=0$. Knowing $D(x,t)$, then $U(x,t)$ can be found using the relation

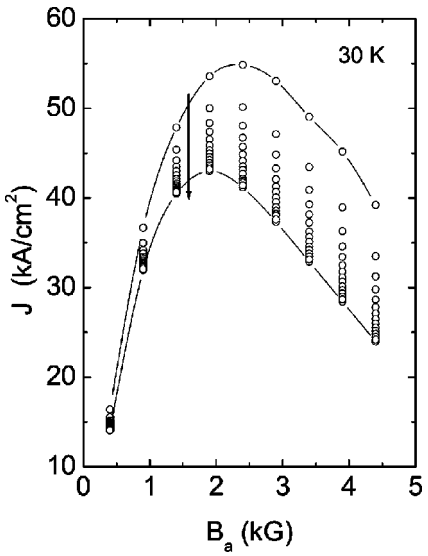

FIG. 3. Persistent current J for the BSCCO (Pb=0.4) crystal as a function of field and time at $T=30$ K. Arrow indicates time evolution. The earliest time corresponds to $t=8$ sec while the longest time is $t=650$ sec.

$$\frac{U}{kT}=-\ln\left(\frac{c\,\eta D}{\phi_0 ABJ}\right), \tag{2}$$

where η is the viscosity coefficient,[40] $A\approx 1$ is a numerical factor, ϕ_0 is the flux quantum, and c the speed of light.

Figure 4 shows the relaxation behavior of U near the sample center as a function of J for various applied fields at 30 K. There is a distinct crossover in the slope of U versus J as B_a is increased beyond the second peak maximum at 2.4 kG. It is also clear from Fig. 4 that for constant current density J the activation energy U is growing with B_a for $B_a<B_{peak}$, and U is decreasing with B_a for $B_a>B_{peak}$.

In Fig. 5, U is plotted as a function of time for the same B_a values presented in Fig. 4. Note that U is approximately linear with the logarithm of the time, in agreement with the logarithmic solution[41,42]

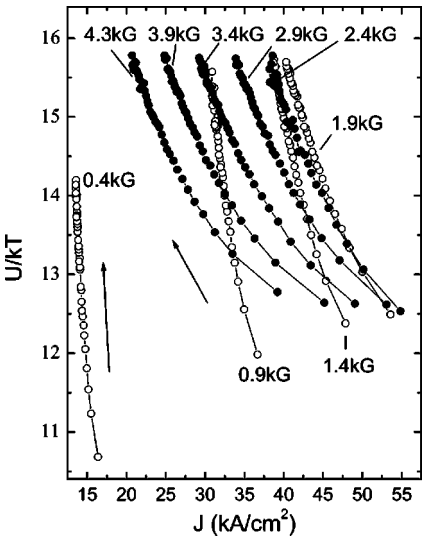

FIG. 4. Barrier energy U as a function of current density J at $T=30$ K for different applied fields during relaxation. Arrows indicate time evolution.

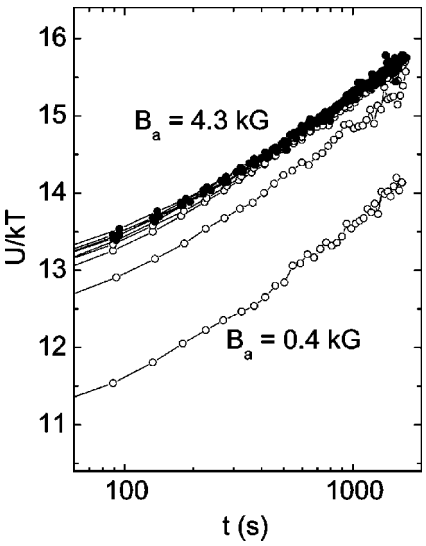

FIG. 5. Temporal development of U at $T=30$ K for different applied fields $B_a=0.4,0.9,1.4,1.9,2.4,2.9,3.4,3.9,4.3$ kG showing data collapse for fields close to and above the peak field.

$$U=kT\ln(t/t_0). \tag{3}$$

In this equation the time scale t_0 in the logarithmic term is proportional to $1/[B_a(\partial U/\partial j)]$, implying that U is only weakly dependent on the applied field B_a, in agreement with the experimental data of Fig. 5.

IV. DISCUSSION

The results of several studies support the conclusion that increasing lead content in $Bi_{2-x}Pb_xSr_2CaCu_2O_{8+\delta}$ will dramatically reduce the anisotropy γ.[29,30] Régi *et al.*[43] showed that after Pb doping the normal-state resistivity along the *c* axis decreases by two orders of magnitude near T_c.[29] In contrast to this, these studies found that the resistivity in the *ab* plane is hardly changed. Other investigations show that the *c*-axis critical current density is also increased by Pb doping.[43] The Josephson coupling energy, which is related to the interlayer coupling strength, was measured to be a factor of 3.5 higher in a maximally doped BSCCO (Pb=0.4) sample.[44] These results all indicate that γ decreases significantly with increasing Pb doping up to the saturation level of BSCCO (Pb=0.4).

Based on studies of deoxygenated YBCO, a scaling relation between γ^2 and B_{irr} has been suggested.[45] There is further evidence that this relation may be universally valid for all high-temperature superconducting materials.[31] By comparing B_{irr} for BSCCO, LSCO, and YBCO, Kitazawa *et al.* extracted the scaling law

$$B_{irr}\approx 3.34\times 10^7\gamma^{-2}\tau^{1.13}, \tag{4}$$

where $\tau=1-T/T_c$ is the reduced temperature and B_{irr} is in Gauss. This empirical relation is used here to fit γ to our B_{irr} data in the range $\tau>0.6$ (see Fig. 7). Also shown in Fig. 6 are data obtained for deoxygenated[46] and optimally oxygen-doped YBCO.[11] For all four crystals the empirical law gives an excellent description of the behavior in the entire temperature range. Fitting the data of Fig. 6 using Eq. (4), the following anisotropy values are determined: BSCCO (Pb=0) $\gamma=270\pm 20$, BSCCO (Pb=0.4) $\gamma=68\pm 5$, YBCO ($\delta=0.5$) $\gamma=45\pm 5$, YBCO ($\delta=1$) $\gamma=12\pm 2$. Provided that the scaling law (4) is correct, these results demonstrate that it is indeed possible to bridge the anisotropy gap between YBCO and BSCCO by Pb doping BSCCO from one side and deoxygenating YBCO from the other.

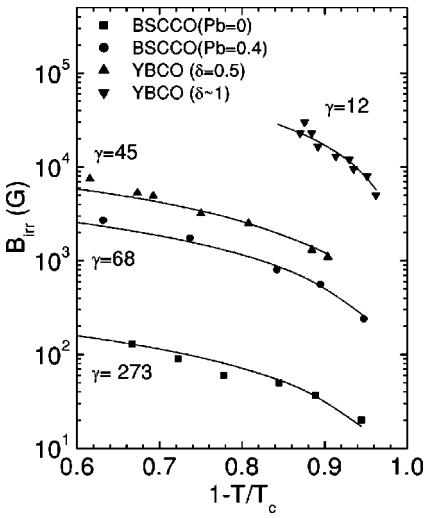

FIG. 6. B_{irr} data of all four crystals as functions of reduced temperature. Shown as full lines are fits by Eq. (3) resulting in the indicated values for γ.

We discuss now the possibility that the second peak is formed due to a vortex matter crossover from three-dimensional (3D) flux-line lattice to a 2D flux structure, as proposed by several authors.[14,31] The predicted crossover field for the 3D-2D transition is given by

$$B_{2D}=\Phi_0/s^2\gamma^2, \tag{5}$$

where s is the interlayer spacing.[47] Between the Pb-doped BSCCO and the deoxygenated YBCO crystals we have a pair of samples, BSCCO (Pb=0.4) and YBCO ($\delta=0.5$), with very different interlayer spacing but similar anisotropy providing the opportunity to compare the B_{peak} with the prediction for B_{2D} over a large temperature range.

Figure 7 shows a plot of the B_{peak} fields of both YBCO crystals, the ''pure'' BSCCO and the Pb-doped BSCCO crystals. Using $s=0.43$ nm for YBCO and $s=1.54$ nm for

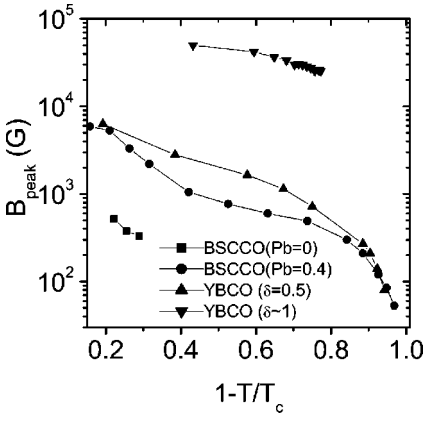

FIG. 7. B_{peak} of all four crystals as functions of reduced temperature.

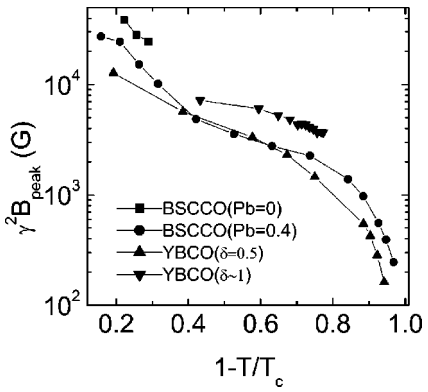

FIG. 8. Plots of $\gamma^2 B_{peak}$ versus reduced temperature for the four crystals.

BSCCO together with the γ values found by the above empirical method, very little correlation is found between the values of B_{peak} and B_{2D}. As an example, using Eq. (5) for YBCO ($\delta=0.5$) a value of $B_{2D}=50$ kG is estimated and for BSCCO (Pb=0.4) $B_{2D}=1.8$ kG, but the graph shows peak fields for these two samples much closer in value. This leads to the conclusion that the 3D-2D decoupling mechanism is not responsible for the second peak.[48]

The results, in fact, suggest another relation for B_{peak} independent of s, i.e., $B_{peak} \propto \gamma^{-2}$. This is supported by the graphs shown in Fig. 8, where $\gamma^2 B_{peak}$ is plotted against the reduced temperature for all four crystals. The four curves deviate by less than a factor of two over a wide temperature range, $\tau=0.4-0.8$. Hence both the irreversibility field and the second peak fields seem to be governed by the anisotropy.

An analysis of the relaxation data shows that the peak field is moving with time to lower values (see Fig. 3). This points to a dynamic origin of the peak, which is further strengthened by the shape of the $U(J)$ curve as a function of field. The slope $\partial U/\partial J$ is different before and after the peak, which is consistent with a different relaxation process in either of the two field ranges.[10] In the dynamic model the peak is formed as the relaxation speeds up after the peak field is reached, thus decreasing $J(t)$. The dynamic picture is also consistent with results by Yeshurun *et al.*[6] and by Tamegai *et al.*[49] showing a clear time dependence of the second peak in BSCCO. Both studies show that the peak is virtually absent when the loops are measured on a short time scale while the peak gradually appears as the time scale is expanded. As pointed out in the previous section, the activation energy grows with B below the second peak and decreases after the peak. This crossover in the field dependence indicates an *elastic-to-plastic creep crossover* around the peak-field similar to that observed in $NbSe_2$,[20], YBCO,[10] NCCO,[12] BSCCO,[22,23] TBCCO,[16,23] and HBCO.[17]

A natural explanation is found within the framework of the elastic-to-plastic creep crossover scenario for the fact that $B_{peak} \propto \gamma^{-2}$. To roughly estimate the crossover field and equate the values of the elastic and plastic pinning barriers,[10] the following relation can be used:

$$\frac{\epsilon_0}{\gamma\sqrt{B_p}} \sim kT \ln(t/t_0), \tag{6}$$

where $\epsilon_0=(\Phi_0/4\pi\lambda)^2$ is the vortex tension. For a constant time window t, determined by the experimental technique, Eq. (6) yields

$$B_p \propto \gamma^{-2}. \tag{7}$$

An important feature in the magnetization curves of Fig. 1 is the onset-field B_{on} of the anomalous second peak in the magnetization curve. The field B_{on} is plotted in Fig. 2 for the BSCCO (Pb=0.4) crystal. Consistent with recent experimental work[11,12] it is shown below that the line $B_{on}(T)$ separates two solid vortex phases. The theoretical basis for this claim is as follows. The vortex phase diagram is determined by the interplay between three energy scales: the vortex elastic energy $E_{elastic}$, the energy of thermal fluctuations $E_{thermal}$, and the pinning energy $E_{pinning}$. The competition between the first two determines the melting line[34,50] while the competition between the last two determines the irreversibility line, i.e., the line $B_{on}(T)$ is the intersection of $E_{elastic}(B,T)$ and $E_{pinning}(B,T)$ surfaces. Most relevant to the present work is the competition between the elastic energy and the pinning energy: at low fields the elastic interactions govern the structure of the vortex solid, forming a quasiordered lattice. Above B_{on}, however, disorder dominates and vortex interactions with pinning centers resulting in an entangled solid where cells of the vortex lattice are twisted and dislocations proliferate.

The elastic energy near the solid-entanglement transition, is given by[24,25]

$$E_{elastic}=\epsilon_0 c_L^2 a_0/\gamma, \tag{8}$$

where $a_0=(\Phi_0/B)^{1/2}$ is the intervortex spacing and $c_L \approx 0.1-0.4$ is the Lindemann number. In order to equate $E_{pinning}$ with $E_{elastic}$ it is important to take into account three possible regimes for the pinning energy. These regimes are defined by the three length scales in the problem: the interlayer spacing s, the characteristic size of the longitudinal fluctuations in a cage $L_0 \simeq 2a_0/\gamma$, see also Ref. 51, and the size of a coherently pinned segment of the vortex. The Larkin length is given by $L_c=[\epsilon_0^2 \xi^2/(\gamma^4 \delta_{dis})]^{1/3}$, where δ_{dis} the disorder parameter, and ξ, λ are the coherence length and the penetration depth, respectively. For a 2D case ($L_c<s<L_0$),[24] $E_{pinning}$ becomes

$$E_{pinning} \simeq U_p (L_0/s)^{1/5}. \tag{9}$$

For a 3D case ($s<L_c$),[24,25] if ($L_c<L_0$), it becomes

$$E_{pinning} \simeq U_{dp} (L_0/L_c)^{1/5}, \tag{10}$$

whereas for the case $s<L_0<L_c$,[24]

$$E_{pinning} \simeq \sqrt{\delta_{dis} L_0}, \tag{11}$$

where $U_p=\pi\sqrt{\delta_{dis} s}$ is one pancake pinning energy and $U_{dp}=(\delta_{dis}\epsilon_0 \xi^4/\gamma^2)^{1/3}$ the single vortex depinning energy. The equation

$$E_{elastic}(B,T)=E_{pinning}(B,T) \tag{12}$$

yields the temperature dependence of the onset of the phase transition $B_{on}(T)$ in each of these three regimes.

The curve $B_{on}(T)$ for BSCCO (Pb=0.4) is identified by the open squares in Fig. 2. We consider now the $B_{on}(T)$

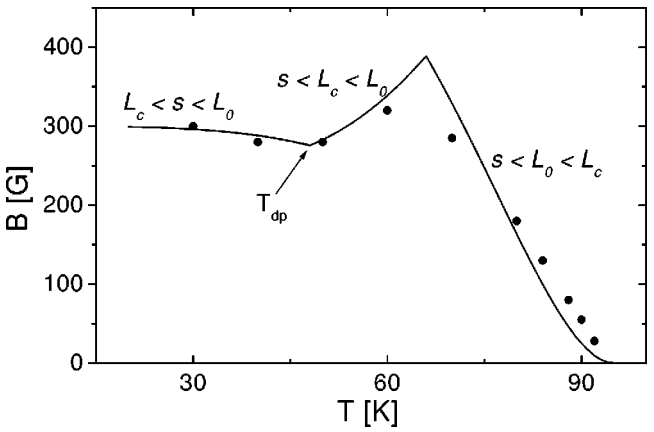

FIG. 9. Second peak onset field B_{on} versus temperature for the BSCCO (Pb=0.4) crystal (circles) shown together with a theoretical curve $E_{elastic}=E_{pinning}$ for different pinning regimes (solid lines).

dependence in the temperature range $25<T<T_c$, where it is not influenced by the interference with the ''first peak'' (see previous section). The line $B_{on}(T)$ is composed of three regimes: (i) B_{on} initially decreases with T; (ii) B_{on} then slightly increases with T, exhibiting a maximum; and finally (iii) B_{on} decreases again up to T_c. It can be shown that these three regimes are directly related to the three $E_{pinning}$ regimes outlined above. First note that L_0 is temperature independent and, for fields of order B_{on} (several hundred Gauss), L_0 is larger than the interlayer spacing $s=1.54$ nm. (For example, for $B=300$ G, $L_0\approx 7.6$ nm.) Inserting the value of the anisotropy obtained above ($\gamma=68$), and reasonable values for ξ (1–10 nm) and λ (100–200 nm), it follows that $L_c \ll 1$ nm at low temperatures. It is therefore possible to conclude that at low temperatures we are in the limit of 2D pinning. Then, substituting Eqs. (9) and (8) into Eq. (12) one obtains[52]

$$B_{on}(T)\propto \xi^{-5/2}=B_{on}(0)[1-(T/T_c)^4]^{5/4}. \tag{13}$$

The fit of this expression to the experimental data for $25<T<48$ K is shown in Fig. 9. Around 48 K, B_{on} starts increasing with temperature. For none of the parameters in Eq. (9) can the temperature dependence change in such a way that B_{on} will start increasing. It therefore seems reasonable to conclude that at around 48 K there is a crossover to a regime where L_c exceeds the value of s. A mechanism which may explain such an abrupt increase in L_c is the temperature smearing of the pinning when the transverse thermal fluctuations of the flux lines become larger than ξ. This occurs at the single vortex depinning temperature.[28] Our experimental results suggest that for BSCCO (Pb=0.4), $T_{dp}\approx 48$ K. Above this temperature the Larkin pinning length starts growing exponentially as given by[25,28]

$$L_c \rightarrow L_c(T_{dp}/T)\exp[(T/T_{dp})^3-1] \tag{14}$$

as a result of a thermal smearing of the quenched disorder. Indeed, our calculations show that in the vicinity of $T\approx 48$ K, $L_c\simeq 1$ nm and becomes of order s. This growth causes a crossover to a regime where $s<L_c<L_0$ and $B_{on}(T)$ is then determined by substituting Eqs. (8) and (10) into Eq. (12). A fit of $B_{on}(T)$ in the temperature range $48<T<66$ K yields the line described in Fig. 9. In this regime B_{on} is predicted to increase with temperature. The decrease of B_{on} with temperature above $T\approx 66$ K implies that at this temperature L_c exceeds the value of L_0. Indeed, our calculations show that in the vicinity of 66 K, $L_c\approx L_0\approx 5$ nm, implying the validity of Eq. (11) for $E_{pinning}$. A fit of the B_{on} data for $T>66$ K, based on Eq. (11), is also shown in Fig. 9.

Finally we note that in the case of ''pure'' BSCCO (Pb =0), $B_{on}(T)$ is approximately constant, in agreement with previous reports.[7,11,12] This constant value is a result of the fact that B_{on} in this material is found only at low temperatures (i.e., $T\ll T_c$) where the superconducting parameters are almost temperature independent. The onset field and the anomalous second peak disappear all together at higher temperatures, because the thermal energy starts to dominate the elastic and the pinning energies.

We also note that in the model of disorder-induced transition B_{on} at $T=0$ must strongly depend on γ.[24,25] Nevertheless in BSCCO (Pb=0.4) its value is the same order of magnitude as in BSCCO (Pb=0). This may be related to a significant increase in disorder parameter δ_{dis} (associated with pinning strength) due to Pb doping.[30] Alternatively, this may be related to the electromagnetic interaction between pancakes in weakly coupled layered superconductors; when this interaction is taken into account,[55] a *similar* value for the disorder parameter δ_{dis} may be used for BSCCO (Pb=0) as for BSCCO (Pb=0.4) to obtain a value of 200 G for $B_{on}(T=0)$ in BSCCO (Pb=0).

V. SUMMARY AND CONCLUSIONS

The B-T phase diagram of Pb-doped and Pb-free BSCCO has been measured and it was found that doping dramatically changes the characteristic fields. For the undoped crystal a second magnetization peak in the temperature interval 20–26 K was observed while the doped sample exhibited a second peak over the entire temperature range, 15–92 K. Furthermore, the irreversibility field increases by an order of magnitude in the doped sample as compared to the undoped crystal over the entire temperature range. The overall B-T properties of the Pb-doped sample approaches those of deoxygenated YBCO. Using a recently proposed scaling expression, the anisotropy values $\gamma_{[BSCCO(Pb=0)]}=270\pm 20$, $\gamma_{[BSCCO(Pb=0.4)]}=68\pm 5$, and $\gamma_{[YBCO(0.5)]}=45\pm 5$, were determined.

Based on these anisotropy values our data show that the relation $B_{2D}=\Phi_0/s^2\gamma^2$ is not appropriate to describe the position of the second peak, showing that the second peak is not due to a 3D-2D decoupling. Instead we find that $B_{peak}\propto\gamma^{-2}$ is an excellent description of the behavior for the two YBCO and the doped BSCCO crystals in complete agreement with the elastic-to-plastic creep crossover scenario, which is also evident from our independent relaxation measurements.

In addition, the B_{on} field is shown to be an onset of the vortex entanglement transition. An excellent fit of the experimental $B_{on}(T)$ data was found, with three basic regimes: $L_c<s<L_0$ for $T<48$ K, $s<L_c<L_0$ for $48<T<66$ K, and $s<L_0<L_c$ for $T>66$ K.

ACKNOWLEDGMENTS

Financial support was provided by the Norwegian Research Council and the University of Oslo. This research was also partially supported by The Israel Science Foundation founded by the Israel Academy of Sciences and Humanities-Center of Excellence Program, and by the Heinrich Hertz Minerva Center for High Temperature Superconductivity. Y.Y. acknowledges the support from the U.S.-Israel Binational Science Foundation. D.G. acknowledges support from the Clore Foundation. M.M. acknowledges support of the U.S.A.-Israel Binational Science Foundation, and of the Director of Energy Research, Office of Basic Energy Sciences through the Midwest Superconductivity Consortium (MISCON) DOE Grant No. DE-FG02-90ER45427.

[1] R. Cubitt, E.M. Forgan, G. Yang, S.L. Lee, D.M. Paul, H.A. Mook, M. Yethiraj, P.H. Kes, T.W. Li, A.A. Menovsky, Z. Tarnawski, and K. Mortensen, Nature (London) **365**, 407 (1993).

[2] S.L. Lee, P. Zimmermann, H. Keller, M. Warden, I.M. Savic, R. Schauwecker, D. Zech, R. Cubitt, E.M. Forgan, P.H. Kes, T.W. Li, A.A. Menovsky, and Z. Tarnawski, Phys. Rev. Lett. **71**, 3862 (1993).

[3] V.N. Kopylov, A.E. Koshelev, I.F. Schegolev, and T.G. Togonidze, Physica C **170**, 291 (1990).

[4] N. Chikumoto, M. Konczykowski, N. Motohira, and A.P. Malozemoff, Phys. Rev. Lett. **69**, 1260 (1992).

[5] T. Tamegai, Y. Iye, I. Oguro, and K. Kishio, Physica C **213**, 33 (1993).

[6] Y. Yeshurun, N. Bontemps, L. Burlachkov, and A. Kapitulnik, Phys. Rev. B **49**, R1548 (1994).

[7] B. Khaykovich, E. Zeldov, D. Majer, T.W. Li, P.H. Kes, and M. Konczykowski, Phys. Rev. Lett. **76**, 2555 (1996).

[8] V.K. Vlasko-Vlasov, G.W. Crabtree, U. Welp, and V.I. Nikitenko, in *Physics and Materials Science of Vortex States, Flux Pinning and Dynamics*, Vol. 356 of *NATO Advanced Study Institute, Series E: Applied Sciences*, edited by R. Kossowsky, S. Bose, V. Pan, and Z. Duruzoy (Kluwer, Dordrecht, 1999), p. 205.

[9] M. Daemling, J.M. Seutjens, and D.C. Laralestier, Nature (London) **346**, 332 (1990); L. Klein, E.R. Yacoby, Y. Yeshurun, A. Erb, G. Muller-Vogt, V. Breit, and H. Wuhl, Phys. Rev. B **49**, 4403 (1994); L. Krusin-Elbaum, L. Civale, V.M. Vinokur, and F. Holtzberg, Phys. Rev. Lett. **69**, 2280 (1992).

[10] Y. Abulafia, A. Shaulov, Y. Wolfus, R. Prozorov, L. Burlachkov, Y. Yeshurun, D. Majer, E. Zeldov, H. Wühl, V.B. Geskenbein, and V.M. Vinokur, Phys. Rev. Lett. **77**, 1596 (1996).

[11] D. Giller, A. Shaulov, Y. Yeshurun, and J. Giapintzakis, Phys. Rev. B **60**, 106 (1999); D. Giller, J. Giapintzakis, A. Shaulov, and Y. Yeshurun, Physica B **284-8**, 697 (2000).

[12] D. Giller, A. Shaulov, R. Prozorov, Y. Abulafia, Y. Wolfus, L. Burlachkov, Y. Yeshurun, E. Zeldov, and V.M. Vinokur, J.L. Peng, and R.L. Greene, Phys. Rev. Lett. **79**, 2542 (1997).

[13] Y.V. Bugoslavsky, A.L. Ivanov, A.A. Minakov, and S.I. Vasyurin, Physica C **233**, 67 (1994); M. Okuya, T. Sasagawa, H. Ikuta, J. Shimoyama, K. Kitazawa, and K. Kishio, *ibid.* **282**, 2239 (1997).

[14] V. Hardy, A. Wahl, A. Ruyter, A. Maignan, C. Martin, L. Coudrier, J. Provost, and C. Simon, Physica C **232**, 347 (1994).

[15] A. Maignan, S.N. Putilin, V. Hardy, C. Simon, and B. Raveau, Physica C **266**, 173 (1996).

[16] T. Aouaroun and C. Simon, Physica C **306**, 238 (1998).

[17] M. Pissas, D. Stampoulos, E. Moraitakis, G. Kallias, D. Niarchos, and M. Charalambous, Phys. Rev. B **59**, 12 121 (1999).

[18] S.B. Roy and P. Chaddah, Physica C **279**, 1 (1997).

[19] G. Ravikumar, V.C. Sahni, P.K. Mishra, T.V.C. Rao, S.S. Banerjee, A.K. Grover, S. Ramakrishnan, S. Bhattacharya, M.J. Higgins, E. Yamamoto, Y. Haga, M. Hedo, Y. Inada, and Y. Onuki, Phys. Rev. B **57**, R11 069 (1998).

[20] S. Bhattacharya and M.J. Higgins, Phys. Rev. Lett. **70**, 2617 (1993).

[21] P.L. Gammel, U. Yaron, Y.P. Ramirez, D.J. Bishop, A.M. Chang, R. Ruel, L.N. Pfeiffer, E. Bucher, G. D'Anna, D.A. Huse, K. Mortensen, M.R. Eskildsen, and P.H. Kes, Phys. Rev. Lett. **80**, 833 (1998).

[22] J.T. Totty, G.K. Perkins, H.J. Jensen, R.A. Doyle, and L.F. Cohen, Supercond. Sci. Technol. **11**, 866 (1998).

[23] R. Griessen, A.F.T. Hoekstra, H.H. Wen, G. Doornbos, and H.G. Schnack, Physica C **282**, 347 (1997).

[24] V. Vinokur, B. Khaykovich, E. Zeldov, M. Konczykowski, R.A. Doyle, and P.H. Kes, Physica C **295**, 20 (1998).

[25] D. Ertaş and D.R. Nelson, Physica C **272**, 79 (1996).

[26] T. Giamarchi and P. Le Doussal, Phys. Rev. B **55**, 6577 (1997); J. Kierfeld, Physica C **300**, 171 (1998); T. Giamarchi and P. Le Doussal, Phys. Rev. Lett. **72**, 1530 (1994); J. Kierfeld, T. Nattermann, and T. Hwa, Phys. Rev. B **55**, 626 (1997).

[27] S. Ooi, T. Tamegai, and T. Shibauchi, J. Low Temp. Phys. **105**, 1011 (1996).

[28] G. Blatter, M.V. Feigel'man, V.B. Geshkenbein, A.I. Larkin, and V.M. Vinokur, Rev. Mod. Phys. **66**, 1125 (1994).

[29] F.X. Régi, J. Schneck, H. Savary, R. Mellet, and C. Daguet, Appl. Supercond. **1**, 627 (1993).

[30] I. Chong, Z. Hiroi, M. Izumi, J. Shimoyama, Y. Nakayama, K. Kishio, T. Terashima, Y. Bando, and M. Takano, Science **276**, 770 (1997).

[31] K. Kitazawa, J. Shimoyama, H. Ikuta, T. Sasagawa, and K. Kishio, Physica C **282**, 335 (1997).

[32] J. Schneck and L. Pierre, Phase Transit. **30**, 139 (1991).

[33] J. Shimoyama, Y. Nakayama, K. Kitazawa, K. Kishio, Z. Heroi, I. Chong, and M. Takano, Physica C **281**, 69 (1997).

[34] E. Zeldov, D. Majer, M. Konczykowski, V.B. Geshkenbein, V.M. Vinokur, and H. Shtrikman, Nature (London) **375**, 373 (1995).

[35] T.H. Johansen, M. Baziljevich, H. Bratsberg, Y. Galperin, P.E. Lindelof, Y. Shen, and P. Vase, Phys. Rev. B **54**, 16 264 (1996).

[36] E.H. Brandt, Rep. Prog. Phys. **58**, 1465 (1995).

[37] T. Schuster, H. Kuhn, and E.H. Brandt, Phys. Rev. B **51**, R697 (1995).

[38] Y. Abulafia, D. Giller, Y. Wolfus, A. Shaulov, Y. Yeshurun, D. Majer, E. Zeldov, J.L. Peng, and R.L. Greene, J. Appl. Phys. **81**, 4944 (1997).

[39] Y. Abulafia, A. Shaulov, Y. Wolfus, R. Prozorov, L. Burlachkov, Y. Yeshurun, D. Mayer, E. Zeldov, and V.M. Vinokur, Phys. Rev. Lett. **75**, 2404 (1995).

[40] The viscosity coefficient $\eta = \phi_0 H_{c2}/c\rho_n \sim 10^{-5}$ g/cm sec was es-

timated using a typical value for the normal-state resistivity of Pb-doped BSCCO $\rho_n \sim 10\ \mu\Omega$ cm (Ref. 30) and a typical value for an upper critical field $H_{c2} \sim 100$ T at $T = 30$ K measured for BSCCO (Ref. 53), assuming that Pb doping does not change H_{c2} considerably. (Note that both crystals have a similar T_c.) Note that the error in the estimation of the η value may only introduce a parallel shift of all the data, being unable to influence qualitative observations.

[41] V.B. Geskenbein and A.I. Larkin, Zh. Éksp. Teor. Fiz. **95**, 1108 (1989) [Sov. Phys. JETP **68**, 639 (1989)].

[42] L. Burlachkov, D. Giller, and R. Prozorov, Phys. Rev. B **58**, 15 067 (1998).

[43] F.X. Régi, J. Schneck, J-F. Palmier, P. Müller, and H. Savary, Physica C **235-240**, 3293 (1994).

[44] L. Winkeler, S. Sadewasser, B. Beschoten, H. Frank, F. Nouvertné, and G. Güntherodt, Physica C **265**, 194 (1996).

[45] L. Hou, J. Deak, P. Metcalf, and M. McElfresh, Phys. Rev. B **50**, 7226 (1994); A. Schilling, R. Jin, H.R. Ott, and Th. Wolf, Physica C **235-240**, 2741 (1994); J. Deak, L. Hou, P. Metcalf, and M. McElfresh, Phys. Rev. B **51**, 705 (1995); L. Hou, J. Deak, P. Metcalf, M. McElfresh, and G. Preosti, *ibid.* **55**, 11 806 (1997).

[46] Shi Li and M. McElfresh (unpublished).

[47] V.M. Vinokur, P.H. Kes, and A.E. Koshelev, Physica C **168**, 29 (1990).

[48] This is consistent with other results, showing a clear dependence of the peak position on the disorder which is not present in the expression for B_{2D}—see, for example, B. Khaykovich, M. Konczykowski, E. Zeldov, R.A. Doyle, D. Majer, P.H. Kes, and T.W. Li, Phys. Rev. B **56**, R517 (1997); T. Nishizaki, T. Naito, S. Okayasu, A. Iwase, and N. Kobayashi, Phys. Rev. B **61**, 3649 (2000).

[49] T. Tamegai, Y. Iye, I. Oguro, and K. Kishio, Physica C **213**, 33 (1993).

[50] A. Schilling, R.A. Fisher, N.E. Phillips, U. Welp, W.K. Kwok, and G.W. Crabtree, Phys. Rev. Lett. **78**, 4833 (1997); H. Safar, P.L. Gammel, D.A. Huse, D.J. Bishop, W.C. Lee, J. Giapintzakis, and D.M. Ginsberg, *ibid.* **70**, 3800 (1993); H. Safar, P.L. Gammel, D.A. Huse, G.B. Alers, D.J. Bishop, W.C. Lee, J. Giapintzakis, and D.M. Ginsberg, Phys. Rev. B **52**, 6211 (1995).

[51] E.H. Brandt, J. Low Temp. Phys. **44**, 33 (1981).

[52] Note that this equation is valid for the case of δT_c pinning (Refs. 12, 28, and 54). Pinning may be caused by spatial fluctuations of T_c (''δT_c pinning'') or of the charge-carrier mean free path l (''δl pinning'') near a lattice defect. Spatial variations of T_c lead to spatial modulation of the linear and quadratic terms in the Ginzburg-Landau (GL) free-energy functional, whereas variations of the mean free path affect the gradient of the order parameter in the GL functional; for further discussion see Ref. 28, p. 1141. In Refs. 11 and 54 we show that a fingerprint of a δT_c pinning is a decrease of B_{on} with T at intermediate temperatures.

[53] A.I. Golovashkin, O.M. Ivanenko, Y.B. Kudasov, K.V. Mitsen, A.I. Pavlovsky, V.V. Platonov, and O.M. Tatsenko, Physica C **185**, 1859 (1991); A.S. Alexandrov, W.Y. Liang, and V.N. Zavaritsky, J. Low Temp. Phys. **105**, 749 (1996).

[54] D. Giller, A. Shaulov, and Y. Yeshurun, Physica B **284-288**, 687 (2000).

[55] A.E. Koshelev and V.M. Vinokur, Phys. Rev. B **57**, 8026 (1998).